The Effects of Collimator Malpositioning in Seven Pinhole Tomography

Neil W. Ratzlaff, Paul H. Brown, Deborah J. Cox, and G.T. Krishnamurthy

VA Medical Center and Oregon Health Sciences University, Portland, Oregon

We tested the effect of seven pinhole collimator positioning on circumferential count profiles during thallium-201 myocardial imaging by imaging a left ventricular phantom at various angles. The seven pinhole raw data images and profiles were identifiable as malpositioned when the collimator was malpositioned by 10° or more. The phantom's "cold" spot was shown to propagate into adjacent planes and also into other regions of the heart as a function of collimator positioning. We then developed a method for systematically positioning the collimator correctly, which should aid in preventing similar artifacts in clinical studies.

Seven pinhole tomography (*1*) has been suggested for imaging myocardial perfusion with Tl-201. Proper collimator positioning is necessary to avoid image artifacts, yet is difficult to obtain because of the low energy of the 68 keV x-rays, the poor target-to-background ratio (*2*), and the geometric distortion inherent in the design of the seven pinhole collimator (*3*). Determination of the correct collimator orientation based on viewing raw data seven pinhole images on the scintillation camera's persistence oscilloscope requires conceptually difficult three-dimensional thought processes, followed by trial-and-error positioning changes, or the use of simple rules to decide how to change the collimator position. We undertook a study to measure the effect of malpositioning in final data analysis and to devise some simple rules for correct collimator positioning.

Methods

We used a cardiac phantom previously used by investigators to simulate the myocardial wall in a study of the accuracy of tomographic reconstruction (*4*). (This previous study did not consider effects due to collimator positioning.) It was a bullet-shaped Lucite phantom that has a rounded nose (the cardiac apex) and a cylindrical body (9 cm diameter, 13 cm high). The cylindrical central chamber represents the ventricular blood cavity, and an outer ring represents the myocardial wall (1.5 cm thick). The central chamber was filled with water, as was a 90° segment (24 cc) of the outer ring to represent a myocardial wall perfusion defect. The remaining 270° segment of the outer ring was filled with 1.2 mCi of Tl-201 to simulate the normal myocardial wall. Thus, a tomographic slice through the defect (which was only 3.2 cm high in the 13 cm high cylinder) should appear as a ring with a 90° cold spot with 0% of maximum counts. A slice above or below the defect should appear as a uniform ring.

The phantom was placed apex upward to represent the left ventricle in the left anterior oblique (LAO) view, with the defect on the "patient's" septal wall. The phantom was placed under a large field scintillation camera with ½ in. crystal, equipped with a seven pinhole collimator with 5-mm pinholes. Using the image from the center view (the correct collimator positioning view, looking directly down the long axis of the phantom) as the starting point, we acquired malpositioned images at 5,10,15, and 20° angles in caudal, LAO, and right anterior oblique (RAO) projections. Three center images were acquired at different times. For each camera angle, the phantom was moved along the horizontal plane to center the image in the field of view with no clipping of the outer six images. In addition, distance from the collimator to the phantom was adjusted so that the central pinhole image filled to about 75% of its field of view. A 40% energy window centered on 68-keV Hg-201 x-rays (*5*) was used to acquire 400,000 counts in each image in a 128 × 128 byte matrix.

A computer reconstruction algorithm (*6*) was used to produce twelve tomographic slices through the phantom, with a nominal 1-cm thick plane at 12 cm from the collimator face. A circle profile analysis (*7*) starting at 12 o'clock and normalized to maximum pixel counts in the slice was generated for each of the three slices through the mid-height of the phantom as identified by the slices that best showed the defect. The circle profile curves from the three center views were averaged, and this average curve was labeled "true." The curves generated from the circle profiles on the images from other angles were compared to this true curve.

For reprints contact: P.H. Brown, VA Medical Center (115P), 3710 SW US Veterans Hospital Road, Portland, OR 97201.

To investigate the effect of photon energy on this type of experiment, a center view was also acquired using Tc-99m at 140 keV.

Results and Discussion

Perfect Positioning: Figure 1(A) shows the center view raw data when the phantom is perfectly positioned. The central pinhole image is the only image that is circular, and there is shape symmetry between the views on opposing sides of the central image. The intensity of the opposite views is not completely symmetrical due to the presence of the defect on one side. Slices 6 through 9 (slices are numbered from apex to base of phantom) are shown in Fig. 1(B). The defect is best seen in slice 8 and is less well seen in slices 7 and 9. The apparent diameter of the slices decreases as planes are reconstructed farther from the collimator as a result of pinhole geometric distortion. The curves for slices 7 through 9 were identical; the curve for slice 8 is shown along with the true curve in Fig. 1(C). The curve illustrates another problem of seven pinhole tomography: it shows only a 55% defect instead of the correct 0% defect (*4*). The 83% defect at about one o'clock is the result of the 0.5-cm thick partition between two of the myocardial wall chambers at this level of the phantom.

5 to 15° Rotation: The raw data images from any 5° angle were not distinguishable from center images, nor did the circle profile curves deviate by more than a few percent from the true curve. The raw data images with a collimator tilt from center in any direction of 10 or 15° were perceived by several skilled image interpreters as incorrectly positioned due to nonsymmetry of shape of opposite views, and the circle profile through the defect was typically 5% (range 0–10%) different from the true curve. Circle profile curves are generally used clinically by comparing the patient profile to that of a group of normal control subjects (*8*). If the patient profile is already close to the limit of normality, even a small 10–15° angle of malpositioning may be sufficient to cause a false-negative or false-positive result. These profile effects are more obvious with larger angles of malpositioning as we will show.

20° Rotation—Caudal, LAO, RAO: Caudal tilt of 20° produces a raw data image [Fig. 2(A)] that shows incorrect positioning. The image at 12 o'clock is more circular than at 6 o'clock and the pairs of images at 2 and 8 o'clock and 4 and 10 o'clock are not symmetric. The pinhole that produces the image at 12 o'clock is looking most directly down the barrel of the phantom. The position of this pinhole in the collimator is located nearest the patient's feet. To correct the malpositioning the collimator should be tilted in a direction that will cause the central pinhole to face the same direction as the pinhole responsible for the 12 o'clock image. A cephalad tilt is necessary to correct the caudal malposition. If the phantom is centered before the camera is rotated, the phantom must be moved in the horizontal plane after camera rotation to return it to the center of the field of view. The curve generated from slice 8 of the caudal 20° reconstruction is shown in Fig. 2(B) along with the true curve. The magnitude of the caudal 20° defect is the same as the true defect, but it appears to be shifted clockwise. The reconstruction shows a false increase in activity in the inferior edge of the septal defect, which is further away from the collimator surface than the superior edge of the defect, which shows a false decrease in activity. We attribute the increase in the inferior counts in this caudal tilt to a count contribution from the activity in front of slice 8 (i.e., between slice 8 and the collimator), whereas the superior portion is viewed with less overlying activity. Compared to the true curve, this degree of malpositioning can create a false-negative result in the inferior-septal area and a false-positive result in the superior-septal area.

The raw data image from LAO 20° [Fig. 3(A)] also shows incorrect positioning: images at 2 and 4 o'clock are more circular than at 8 and 10 o'clock. Figure 3(B) is the circle profile generated from slice 8 of the reconstruction, very close to the true curve except at the superior edge of the defect. This decrease in activity is caused by the shadow of the chamber partition at 1 o'clock, because the camera has to look from the lateral side through the phantom to see the major defect. In addition to this phenomenon, slice 9 in Fig. 3(C) shows an exaggerated defect depth.

The raw data image from RAO 20° in Fig. 4(A) again shows malpositioning: images at 8 and 10 o'clock are more circular than at 2 and 4 o'clock. Figure 4(B) shows the reconstructed slices 7 through 10. The shapes of slices 7–10 are circular, but the images illustrate the curious artifact of the defect moving

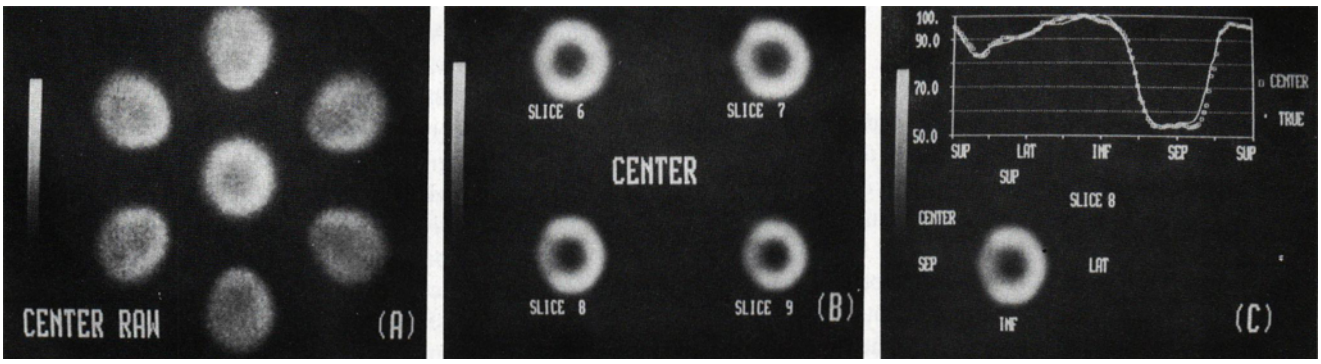

FIG. 1. Data from center view, looking directly down the barrel of the phantom: (A) seven pinhole raw data image, (B) four selected reconstructed tomographic planes with the perfusion defect seen best in slice 8, (C) circumferential profile curve through slice 8 (center) compared to an average curve (true) generated from three separate center images.

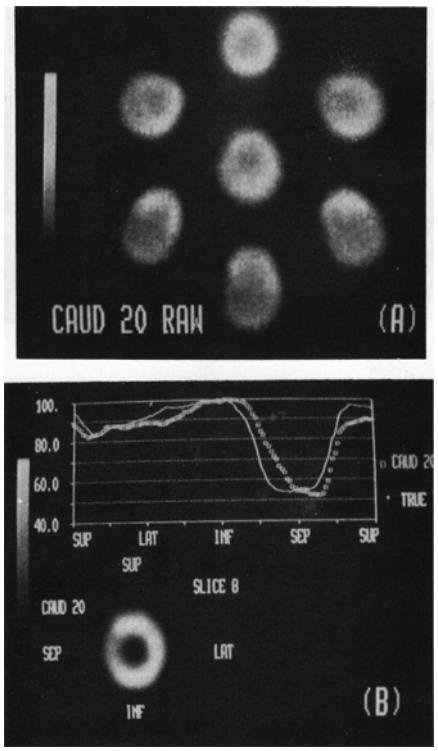

FIG. 2. Data from view malpositioned with a caudal tilt of 20°: (A) raw data and (B) circle profile through plane of the defect compared to true curve.

gradually from the septal side of the phantom in slice 7 to the lateral side in slice 10. The camera is malpositioned on the septal side of the phantom, so by pinhole geometry the defect appears larger than it actually is. In the circle profile for slice 7 [Fig. 4(C)] the defect is shown as wider and deeper than the true defect. Figure 4(D) shows the defect as 40% in slice 8 rather than 30% as in slice 7, but the activity on the left side of the phantom (superior-lateral-inferior) is shown as slightly decreased. The trend continues in slice 9 [Fig. 4(E)]. The defect is close to true, but the apparent activity on the opposite lateral side has been decreased to 20% less than true. This demonstrates that defects artifactually propagate not only into other planes but also into other regions of the heart, as much as 180° removed from the actual defect.

Figure 5(A) sums up the effect of increasing angle on the appearance of the reconstructed defect in the RAO direction for slice 8. The defect appears to become colder with each 5° increase in angle away from center. Figure 5(B) shows the defect differences resulting from viewing the phantom from different directions. The location of the camera in relation to the defect will affect the final evaluation of the defect.

Effect of Photon Energy: The curve from the center image using Tc-99m showed a 20% defect, which was deeper than the 55% defect in the center Tl-201 image [Fig. 1(C)]. Thus at 140 keV the defect measured with seven pinhole tomography is closer to the correct value of 0% than it is for 68 keV. Other positions were not studied with Tc-99m since this radionuclide is not in widespread clinical use for seven pinhole tomography.

Technique for Correct Positioning: It is possible to derive two methods of collimator angle correction from the data we present. One way is to look at the seven images in the raw data image, decide which pinhole is producing the most circular image, and rotate the gamma camera—remember to move the patient in the horizontal plane to maintain a centered image—so that the center pinhole will be looking at the heart from the same direction as the pinhole with the original most circular image did before (*8*). Remember also that the pinhole image is 180° from the pinhole location in the collimator, so the image at the top of the screen is produced by the pinhole nearest the patient's feet. This positioning technique assumes that the heart is radially symmetrical about its long axis.

An easier method is to move the camera toward the direction of the least circular image on the screen: visualize the collimator face as tangent to a sphere centered on the heart and move the camera around the surface of the sphere. Since cameras are not designed to follow such a path, the patient must be moved to compensate for camera rotation. For example, in Fig. 2(A) the image at 6 o'clock is less circular than the image at 12 o'clock, so rotate the camera toward the patient's feet. This will increase the cephalad angle, the proper correction for the caudal angle that produced this image. In Fig. 3(A), incorrect by LAO 20°, proper positioning requires the camera to be moved around the sphere toward the patient's right side. In Fig. 4(A), incorrect by RAO 20°, the images at 2 and 4 o'clock are less circular, so the camera should be moved around the sphere toward the patient's left side. The results using either method of collimator positioning are identical, but the former requires the additional step of knowing which view each pinhole produces and the angle from which it looks.

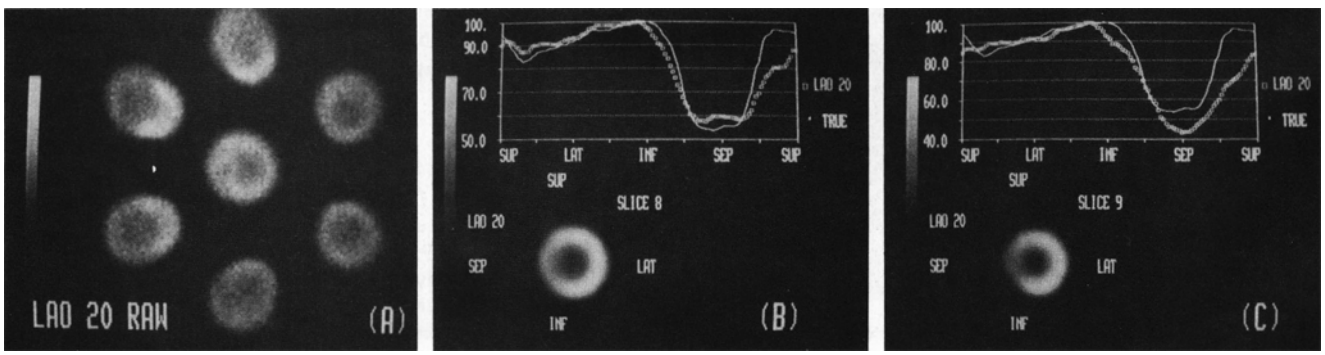

FIG. 3. Data from view malpositioned with a LAO tilt: (A) 20° tilt raw data, (B) circle profile through defect in slice 8 compared to true curve, (C) profile in slice 9.

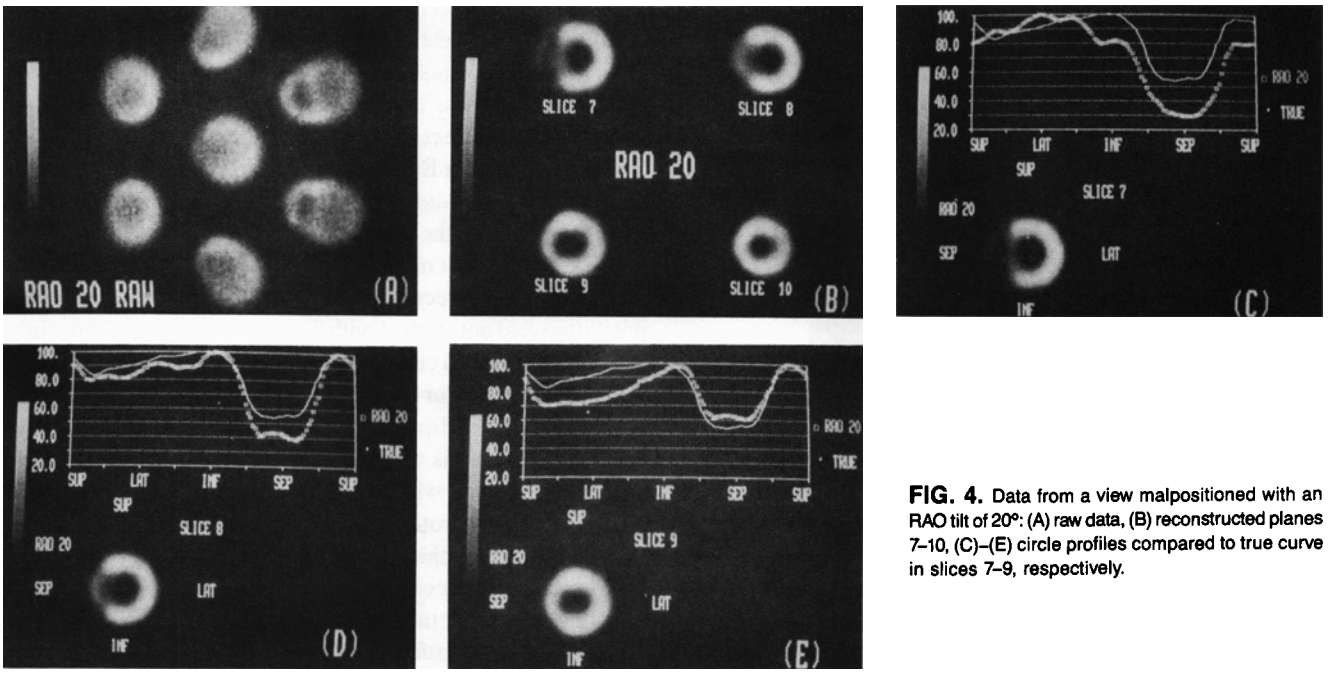

FIG. 4. Data from a view malpositioned with an RAO tilt of 20°: (A) raw data, (B) reconstructed planes 7–10, (C)–(E) circle profiles compared to true curve in slices 7–9, respectively.

We have found our rule of collimator positioning—moving the camera toward the least circular image—to be easy and quick. Rapid collimator positioning is essential to prevent Tl-201 redistribution from obscuring patient defects.

In a patient study, a circular image may not be possible because of the myocardial shape, but opposite views should be symmetric in shape around the center view. Image intensity is affected as a function of viewing angle in relation to the defect location, so image intensity should not be used for positioning. In both Figs. 3(A) and 4(A) the brightest views are on the right side of the patient, but the first is LAO 20° and the second is RAO 20°. The images from a patient may not be as clear as those we show for several reasons, including the lower target-to-background ratio in a clinical study. Blurring of the myocardial image is caused by movement of the heart and scatter from surrounding tissue. For Tl-201, the low energy of the x-rays also contributes to the poor contrast and spatial resolution, which was graphically shown by the 20% defect using Tc-99m compared to the 55% defect using Tl-201. The speed necessary in collimator positioning implies positioning that relies on low count density images obtained with a persistence oscilloscope rather than with the completed 400 K count images we have used. Nevertheless, we have described the results of improper collimator positioning and provided a conceptual description of movements necessary to correct initial positioning. In clinical studies, the sensitivity and specificity for seven pinhole image and curve analysis are typically less than 100% (*8*), which indicates false-positive and false-negative results. A study similar to ours, involving generation of images and profiles in patients at various collimator angles, would be necessary to determine to what extent collimator positioning is responsible for false-positive and false-negative clinical results.

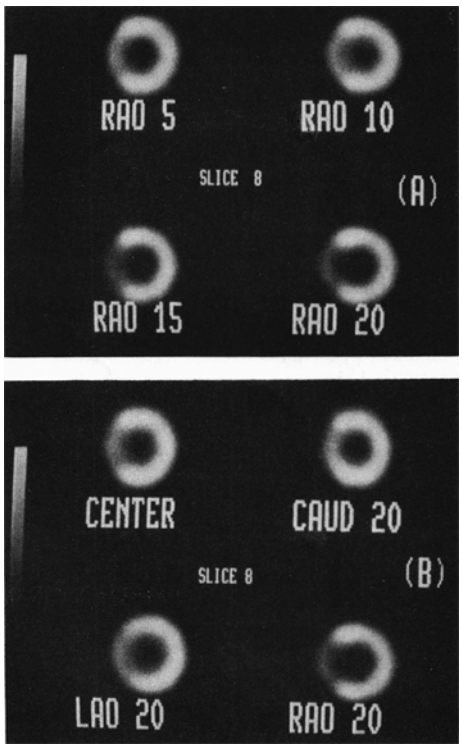

FIG. 5. Summary of effects: (A) effect of increasing angle of RAO malpositioning: 5,10,15, and 20°, (B) effect of various collimator positions: centered, 20° caudal, LAO, and RAO tilt.

References

1. Vogel RA, Kirch DL, LeFree MT, et al. Thallium-201 myocardial perfusion scintigraphy: Results of standard and multi-pinhole tomographic techniques. *Am J Cardiol* 1979;43:787–93.

2. Narahara KA, Hamilton GW, Williams DL, et al. Myocardial imaging with thallium-201: An experimental model for analysis of the true myocardial and background image components. *J Nucl Med* 1977;18:781–86.

3. Vogel RA, Kirch D, LeFree M, et al. A new method of multiplanar emission tomography using a seven-pinhole collimator and an Anger scintilla-

tion camera. *J Nucl Med* 1978;19:648–54.

4. Williams DL, Ritchie JL, Harp GD, et al. In vivo simulation of thallium-201 myocardial scintigraphy by seven-pinhole emission tomography. *J Nucl Med* 1980;21:821–28.

5. Causer DA, Singh H. The effect of gate width on thallium-201 scintigraphy of the myocardium. *Brit J Radiol* 1980;53:142–46.

6. LeFree MT, Vogel RA, Kirch DL, et al. Seven-pinhole tomography—a technical description. *J Nucl Med* 1981;22:48–54.

7. Meade RC, Bamrah VS, Horgan JD, et al. Quantitative methods in the evaluation of thallium-201 myocardial perfusion images. *J Nucl Med* 1978;19:1175–78.

8. Rizi HR, Kline RC, Thrall JH, et al. Thallium-201 myocardial scintigraphy: A critical comparison of seven-pinhole tomography and conventional planar imaging. *J Nucl Med* 1981;22:493–99.